


Mg-based compounds for hydrogen and energy storage

J.-C. Crivello¹ · R. V. Denys² · M. Dornheim³ · M. Felderhoff⁴ · D. M. Grant⁵ ·
J. Huot⁶ · T. R. Jensen⁷ · P. de Jongh⁸ · M. Latroche¹ · G. S. Walker⁵ ·
C. J. Webb⁹ · V. A. Yartys² 

Received: 29 September 2015 / Accepted: 3 January 2016 / Published online: 22 January 2016
© Springer-Verlag Berlin Heidelberg 2016

Abstract Magnesium-based alloys attract significant interest as cost-efficient hydrogen storage materials allowing the combination of high gravimetric storage capacity of hydrogen with fast rates of hydrogen uptake and release and pronounced destabilization of the metal–hydrogen bonding in comparison with binary Mg–H systems. In this review, various groups of magnesium compounds are considered, including (1) RE–Mg–Ni hydrides (RE = La, Pr, Nd); (2) Mg alloys with *p*-elements (X = Si, Ge, Sn, and Al); and (3) magnesium alloys with

d-elements (Ti, Fe, Co, Ni, Cu, Zn, Pd). The hydrogenation–disproportionation–desorption–recombination process in the Mg-based alloys (LaMg₁₂, LaMg₁₁Ni) and unusually high-pressure hydrides synthesized at pressures exceeding 100 MPa (MgNi₂H₃) and stabilized by Ni–H bonding are also discussed. The paper reviews interrelations between the properties of the Mg-based hydrides and *p*–*T* conditions of the metal–hydrogen interactions, chemical composition of the initial alloys, their crystal structures, and microstructural state.

✉ C. J. Webb
j.webb@griffith.edu.au

✉ V. A. Yartys
volodymyr.yartys@ife.no; volodymyr.yartys@gmail.com

J.-C. Crivello
crivello@icmpe.cnrs.fr

R. V. Denys
roman.v.denys@gmail.com

M. Dornheim
martin.dornheim@hzg.de

M. Felderhoff
felderhoff@mpi-muelheim.mpg.de

D. M. Grant
David.Grant@nottingham.ac.uk

J. Huot
jacques.huot@uqtr.ca

T. R. Jensen
trj@chem.au.dk

P. de Jongh
P.E.deJongh@uu.nl

M. Latroche
latroche@icmpe.cnrs.fr

G. S. Walker
Gavin.Walker@nottingham.ac.uk

¹ Université Paris Est, ICMPE (UMR 7182), CNRS, UPEC, 2 rue Henri Dunant, Thiais F-94320, France

² Institute for Energy Technology and Norwegian University of Science and Technology, Kjeller and Trondheim, Norway

³ Helmholtz-Zentrum Geesthacht, Zentrum für Material- und Küstenforschung GmbH, Geesthacht, Germany

⁴ Max-Planck-Institut für Kohlenforschung, Kaiser-Wilhelm-Platz 1, 45470 Mülheim an der Ruhr, Germany

⁵ Nottingham University, Nottingham, UK

⁶ Hydrogen Research Institute, Université du Québec à Trois-Rivières, 3351 Boulevard des Forges, Trois-Rivières, QC, Canada

⁷ Department of Chemistry, Interdisciplinary Nanoscience Center, Aarhus University, Langelandsgade 140, 8000 Aarhus C, Denmark

⁸ Debye Institute for Nanomaterials Science, Utrecht University, Utrecht, Netherlands

⁹ Queensland Micro- and Nanotechnology Centre, Griffith University, Brisbane, Australia

1 Introduction

This work is a review of the recent progress made in the past years, particularly in the framework of the International Energy Agency Task 32 Hydrogen-based Energy Storage, in the area of fundamental and applied studies of Mg-based compounds for hydrogen and energy storage.

In order to find a hydrogen storage system that meets the requirements of low weight (for mobile applications) and adequate capacity, chemical hydrides based on lightweight metals have been extensively investigated [1, 2]. Due to the low cost of extraction from natural chlorides and carbonates which form a significant part of the earth's crust and oceans, magnesium, a lightweight alkaline earth metal, fits many of these requirements.

The reaction of magnesium with hydrogen yields magnesium dihydride (MgH_2) and is reversible, with a storage capacity of 7.6 wt% of hydrogen. The hydrogenation process, however, suffers from slow kinetics, and the dehydrogenation of MgH_2 requires temperatures exceeding 300 °C, which is impracticable for mobile applications and constitutes a significant net energy loss for any system based on MgH_2 .

The kinetics have been shown to improve by crystallite size reduction which allows for shorter hydrogen diffusion paths and the introduction of defects in the material which provides faster pathways for hydrogen to diffuse [3–5]. The introduction of small amounts of additives (typically transition metals and transition metal oxides, but also carbons [6, 7]) has also improved the kinetic rates of absorption and desorption significantly [8]. However, reducing the equilibrium temperature of desorption relies on lowering the thermodynamic enthalpy, and one of the more promising pathways for this is the formation of magnesium alloys with other metals.

Materials suitable for the storage of hydrogen and heat can play an important role for future climate policy goals, because they can compensate for fluctuations in the production of electricity from the renewable energy sources. Of particular interest are metal hydride compounds because these compounds connect energy production and storage with a future hydrogen economy.

Mg-based metal hydrides can be used as solid-state hydrogen storage materials for fuel cell cars, as a hydrogen source for fuel cell auxiliary power units, for the storage of high-temperature heat in industrial processes and in power plants, or for the smoothing of irregular supply of heat and electricity production for fuel cells in domestic energy sectors.

Metal hydrides are produced from different pure metals or metal alloys under the influence of hydrogen. This process of hydrogenation is accompanied by the release of heat (exothermic reaction). The same amount of heat must be supplied to the metal hydride for the decomposition and the release of hydrogen (endothermic reaction, see Eq. 1). These processes are infinitely repeatable, and reversible Mg-based metal hydrides can therefore be used for the storage of heat and hydrogen [9]. Depending on the thermodynamics of the reaction, different temperatures apply to different metal hydrides (Table 1).



1.1 Thermodynamic tuning

The temperature required to generate 1 bar of hydrogen from a hydride system can be calculated from the change in enthalpy and entropy for dehydrogenation, as shown in Eq. 2. Thermodynamic tuning of a multicomponent hydride system requires the addition of a second phase (Z) to the hydride (YH_2), which reacts with the hydride, releasing hydrogen and generating a new alloy or compound (YZ) [12]. As can be seen from Fig. 1, the reduction in the enthalpy for dehydrogenation is determined by the enthalpy of formation for the alloy or compound formed, as shown in Eq. 3.

$$T(1 \text{ bar}) = \Delta H / \Delta S \quad (2)$$

$$\Delta H_b = \Delta H_a + \Delta H_f \quad (3)$$

1.2 Mg alloys with p-elements (X = Al, Si, Ge, Sn)

1.2.1 Silicon

Silicon has a very low solubility in magnesium of 0.003 %. When MgH_2 mixed with Si is heated until the hydrogen is

Table 1 Selected physical data of Mg-based metal hydrides for hydrogen and heat storage applications

Material	H content (wt%)	ΔH_r (kJ/mol H_2)	Heat storage density (kWh/kg)	Equilibrium temperature at 0.1 MPa (°C)	References
MgH_2	7.7	74	0.78	280	[10]
NaMgH_3	4.0	86.6	0.47	380	[11]
Mg_2NiH_4	3.6	62	0.31	250	[10]
Mg_2FeH_6	5.5	77	0.55	320	[10]

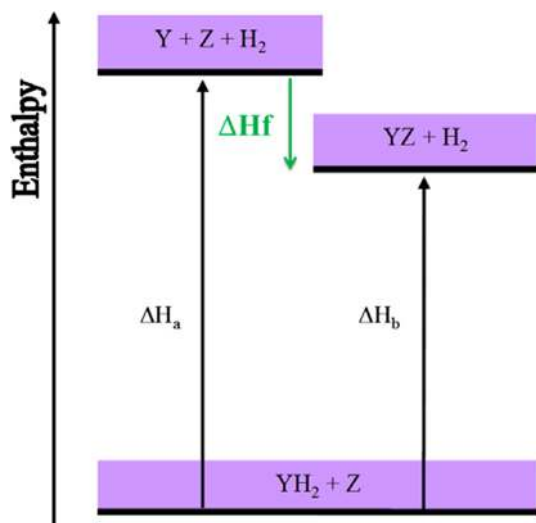


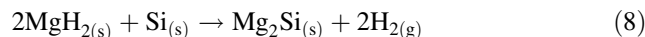
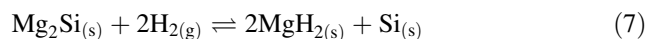
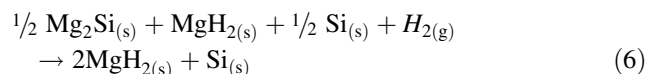
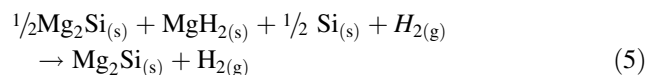
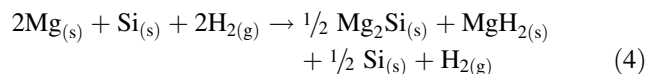
Fig. 1 Thermodynamic tuning for multicomponent systems

released, it forms the intermetallic Mg_2Si [13]. While the reaction is reversible in a ball-mill environment with hydrogen [14–16], application of pressures of hydrogen to Mg_2Si up to 185 MPa and 350 °C has not yielded a hydride phase [13, 17] except when the Mg_2Si particle size was reduced to 10 nm. Even then, the yield was low and the kinetics very poor [18].

Bystrzycki et al. [19] observed only the metastable Mg_5Si_6 in a study of the destabilization of MgH_2 by Si, where Si was deposited by pulsed laser deposition on a MgH_2/Mg substrate and did not find any destabilization.

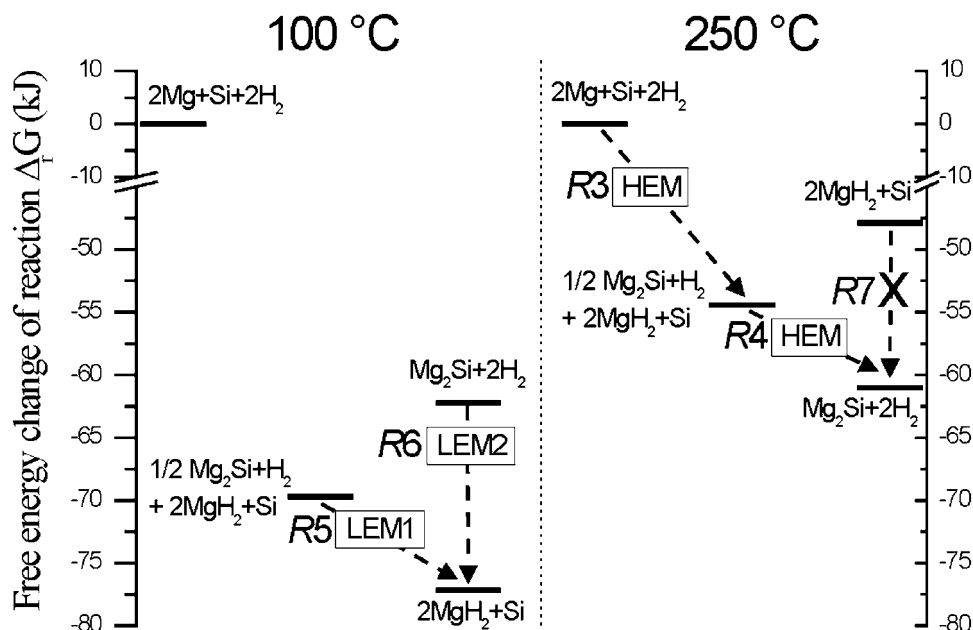
However, the Mg–Si–H system has been studied with regard to its hydrogen storage properties. Samples were

prepared by reactive ball-milling under hydrogen, and depending on the milling conditions, different paths can be obtained. For high rotation speeds, Mg_2Si is formed, whereas $2\text{MgH}_2 + \text{Si}$ are obtained at low rotation speeds. This behaviour can be understood by considering the change in local temperature at the collision impact with milling speed. On this basis, it is observed that the reaction $\text{Mg}_2\text{Si} + 2\text{H}_2 \rightleftharpoons 2\text{MgH}_2 + \text{Si}$ is reversible. The hydrogenation reaction can be achieved by milling Mg_2Si at low rotation speed, whereas the reverse reaction can be triggered by milling at high rotation speed. However, a small quantity of Mg_2Si is necessary to initiate the reaction between magnesium hydride and silicon.



As shown in Fig. 2, starting from the elements, after 4 h of high-energy milling (HEM) under hydrogen, a metastable state is reached where three solid phases coexist (MgH_2 , Si, and Mg_2Si). At this stage, further milling keeping to the HEM regime leads to the formation of Mg_2Si without H_2 absorption, whereas low-energy milling (LEM) allows the formation of $\text{MgH}_2 + \text{Si}$ with full

Fig. 2 Free energy diagrams, showing milling reagents and obtained products for two pressure–temperature conditions (100 and 250 °C at $p(\text{H}_2) = 9 \text{ MPa}$)



hydrogen absorption. It is therefore possible to tune the reaction by switching from HEM to LEM. The final products are dependent on the milling energy which probably governs the local temperature at milling impact (Eqs. 4–8). Interestingly, the full conversion of $\text{Mg}_2\text{Si} + \text{H}_2$ into $\text{MgH}_2 + \text{Si}$ is also possible by LEM. However, the reverse reaction could not be obtained by HEM probably due to kinetic limitations at the MgH_2/Si interfaces. Such limitations are overcome by the presence of Mg_2Si in three-phase mixtures. Contrary to solid/gas reactions, the present work shows that reversible hydrogen storage in Mg_2Si can be achieved by ball-milling at room temperature under moderate hydrogen pressure (9 MPa).

The free-energy change, $\Delta_r G_p^T$, of the reactions observed in this study is displayed in Fig. 2. By increasing the local temperature, the energy level of MgH_2 increases as compared to Mg_2Si . Indeed, the large entropy change associated with the absorption of molecular hydrogen from the gas phase into atomic hydrogen in the Mg lattice accounts for the high variation in $\Delta_r G_p^T$ with temperature. As a consequence, while at low temperatures (e.g. 100 °C) $\Delta_r G_p^T$ is lower for MgH_2 than for Mg_2Si , the opposite occurs at high temperatures (e.g. 250 °C). At the imposed pressure conditions (~ 9 MPa), the crossover temperature is 180 °C. Thus, we argue that under LEM conditions, the reaction temperatures are below 180 °C leading to $\text{MgH}_2 + \text{Si}$ as stable phases. In contrast, local temperatures above 180 °C occur under HEM conditions, and Mg_2Si is produced.

1.2.2 Germanium

Germanium can also be used to reduce the enthalpy of dehydrogenation from MgH_2 , through the formation of magnesium germanide, Mg_2Ge (see Fig. 3) [16]. The enthalpy of formation for Mg_2Ge is 104.6 kJ/mol, which gives an enthalpy of dehydrogenation for $2\text{MgH}_2:\text{Ge}$ of

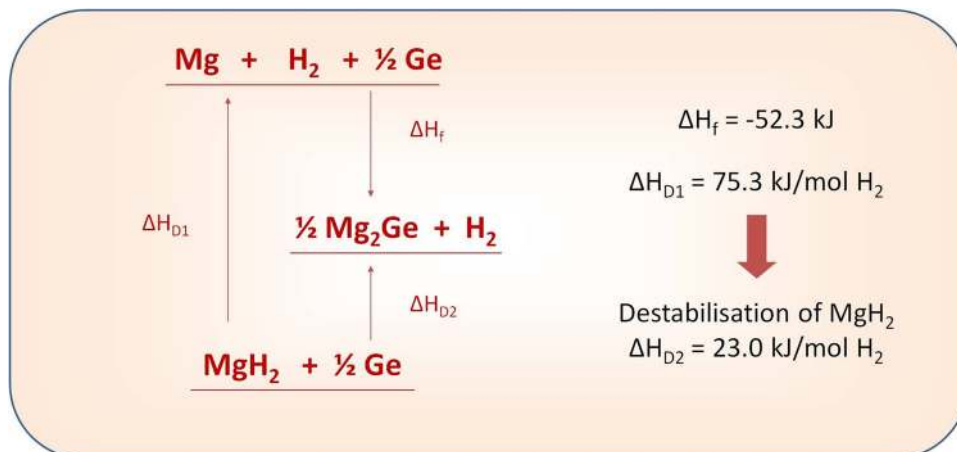
23.0 kJ/mol, yielding a $T(1 \text{ bar})$ of -91.6 °C [20]. Interest in the use of Ge was initially as an additive for improving the kinetics of MgH_2 [21]. Ball-milling the elements Mg and Ge together led to the formation of Mg_2Ge dispersed in a Mg matrix. Unfortunately, the Mg_2Ge was not found to have any positive effect on the hydrogenation of the remaining Mg. Ball-milling MgH_2 with Ge was found to be an effective way to limit the formation of Mg_2Ge phase, but still produces an intimate mixture of the two starting phases [20]. It has also been found that ball-milling MgH_2 and Ge under a hydrogen atmosphere reduces the amount of Mg_2Ge formed even further, presumably through suppressing the formation of Mg metal during milling, which reacts more readily with the Ge [22].

High-pressure DSC results gave a dehydrogenation endothermic peak at 235 °C (regardless of the hydrogen back pressure used, from 0 to 25 bar) [20]. Modifying the sample with a Ti-based additive reduced the dehydrogenation even further, starting at 130 °C (also confirmed in Fig. 4). The kinetics of the reaction were investigated, the unmodified system released hydrogen very quickly at 250 °C, taking only 15 min. Dehydrogenation was more sluggish at 200 °C, only reaching 60 % conversion after 60 min (Fig. 4). However, adding a Ti-based additive gave fast kinetics at 200 °C, with complete conversion within 15 min. These are very favourable results in comparison with the silicide analogues where, after 5 h at 250 °C, the reaction was still not complete for Ti-modified $2\text{Mg}:\text{Si}$ [23].

1.2.3 Tin

Mg_2Sn can be prepared either by powder metallurgy or by ball-milling under an argon atmosphere [16]. Powder metallurgy leads to a cubic antiferroite structure as for Ni and Ge, whereas with ball-milling, a metastable rhombohedral phase is obtained. Such a metastable phase is also

Fig. 3 Destabilization of MgH_2 with Ge [19]



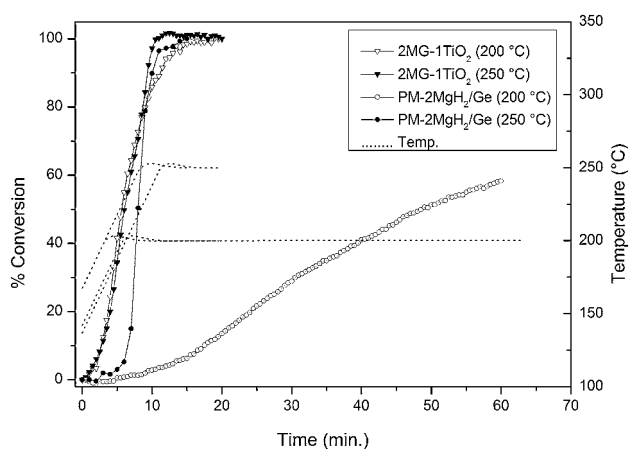


Fig. 4 TGA data for the dehydrogenation of $2\text{MgH}_2/\text{Ge}$ samples with and without a Ti-based additive. Samples were ball-milled for 140 min; TGA used a flowing Ar carrier

observed at high pressure (60 kbar, 900 °C) and is possibly stabilized by a magnesium deficiency leading to the Mg_9Sn_5 stoichiometry instead of the 2:1 ratio. The cubic phase obtained by powder metallurgy was ball-milled under hydrogen gas (20 bar). No hydrogen uptake could be observed, but the formation of the rhombohedral phase occurred in a shorter time (3 h) than milling under argon (12 h). The decomposition of Mg_2Sn was not observed, even for long milling times, but the rapid formation of the rhombohedral phase under hydrogen can be understood by the formation of small quantities of MgH_2 leading to the Mg-deficient Mg_9Sn_5 rhombohedral compound [14].

1.2.4 Aluminium

A sample of $\gamma\text{-Mg}_{17}\text{Al}_{12}$, produced by arc-melting and BM, transformed completely to MgH_2 and metallic Al during hydrogenation ($p(\text{H}_2) = 30$ bar, $T = 350$ °C, $t = 17$ h) [24]. The apparent activation energy for decomposition of air-exposed $\text{MgH}_2\text{-Al}$ is estimated as $E_A \sim 160$ kJ/mol H_2 [24]. This value corresponds to the activation barrier of 160–166 kJ/mol H_2 for the dehydrogenation of pure magnesium hydride [25, 26]. The alloying with Al creates an alloy which is less sensitive towards oxygen contamination and which requires little if any pre-treatment in order to activate [24].

1.3 Magnesium alloys with *d*-elements (Ni, Cu, Co, Ti, Pd, Fe, Zn)

1.3.1 Nickel

The addition of Ni to the Mg system can be beneficial for different reasons. Nickel is a very good (de)hydrogenation catalyst, which means that it facilitates the absorption and

desorption of hydrogen by adsorbing and dissociating hydrogen molecules into adsorbed atomic species and vice versa. It is not necessary to have pure Ni in the system, and Mg–Ni alloys also show these enhanced sorption kinetics [26–28]. For instance, enhanced hydrogen sorption rates, while retaining a high storage capacity of about 6 wt% hydrogen, were obtained for $\text{Mg}_{1-x}\text{Ni}_x$ alloys with different compositions ($0 \leq x \leq 0.33$) prepared by melt spinning [27]. A second aspect is that in the processing of Mg materials, such as ball-milling or nanoconfinement, Ni often has an influence on the structural properties of the resulting material [29].

However, the most important aspect is the possibility to form alloys. The thermodynamic properties for hydrogen desorption from Mg_2NiH_4 are considerably more favourable than those of MgH_2 , with a formation enthalpy for Mg_2NiH_4 of about -64 kJ/mol (decreasing the equilibrium hydrogen desorption temperature under 1 bar H_2 from 300 to 250 °C). Unfortunately, the addition of nickel also significantly reduces the capacity, with Mg_2NiH_4 only containing 3.6 wt% of hydrogen [30].

Recent developments are mostly related to further insight into the properties of Mg_xNi alloys by studying the hydrogenation properties of thin films [31, 32] and nanoparticles, prepared either by supporting on a carbon scaffold [33] or by gas-phase techniques [22, 23]. Using an in situ microscope during hydrogenation, it was possible to visualize the nucleation and growth of Mg_2NiH_4 crystals with a lattice spacing of 0.22 nm in Mg-rich domains, followed by crystallization of MgH_2 , demonstrating how the presence of Mg_2Ni facilitates the hydrogenation of Mg [32]. In addition, measurements on nanoparticles produced by inert gas condensation clearly connected the enhancement of the hydrogen sorption properties to the formation of Mg_2Ni and Mg_2NiH_4 phases [23]. Mg_2Ni , particularly in a form prepared by rapid solidification nanocomposite with Mg [34], enhances the hydrogenation of the Mg-based alloys allowing higher rates of hydrogen absorption and desorption.

Since Ni destabilizes the magnesium–hydrogen bonding, this results in the reduction in the decomposition temperatures of the formed hydrides, as demonstrated for Mg–Mm–Ni alloy-based hydrides nanostructured by Equal Channel Angular Pressing in [35]. The effect of nickel is associated with strong covalent Ni–H bonding which leads to the formation of various types of Ni–H complexes and clusters, $[\text{NiH}_4]^{4-}$ tetrahedra in the case of Mg_2NiH_4 or buckled nets $-\text{Ni}-\text{H}-\text{Ni}-\text{H}-$ penetrating through the structure in the recently studied MgNi_2H_3 [36]. While in both cases the metal sublattice requires a complete rebuilding, for the Laves-type intermetallic MgNi_2 , a hydrogen-induced transformation takes place in the metal sublattice when a very high hydrogen pressure of 28 kbar

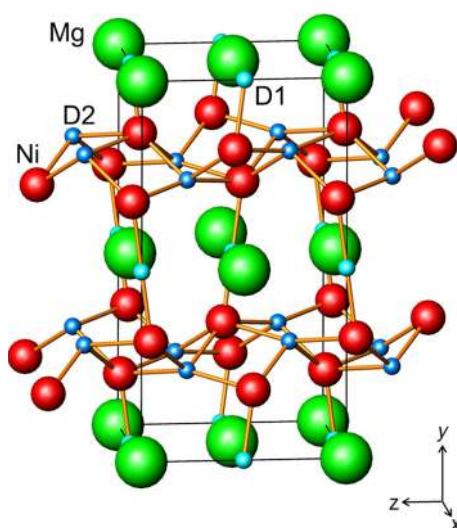


Fig. 5 Crystal structure of MgNi_2D_3 . Two types of sites occupied by deuterium include a Mg_4Ni_2 octahedron for H1(D1) and a chair Ni_4 configuration for H2(D2) located within the buckled Ni–H nets containing bent spirals $-\text{Ni}-\text{H}_2-\text{Ni}-\text{H}_2-$

H_2 is applied at a temperature of 300 °C. Surprisingly, instead of a disproportionation to form MgH_2 , the hydrogenation leads to a rebuilding of the initial hexagonal structure into the orthorhombic distorted MoSi_2 -type sublattice. In the formed MgNi_2H_3 , H atoms fill the deformed octahedra Mg_4Ni_2 and the positions within the buckled nets $-\text{Ni}-\text{H}-\text{Ni}-\text{H}-$ penetrating through the structure (Fig. 5). Analysis of the electronic structure revealed a charge transfer from Mg to Ni, and to the H atoms. The calculated gross heat of formation for the *Cmca* phase of MgNi_2H_3 is ~ 37.3 kJ/mol- H_2 , which is consistent with the stability of the hydride at normal conditions.

1.3.2 Copper

No ternary hydrides have been reported in the literature for the Mg–Cu system. However, the role of copper is to substitute the hydrogen in the MgH_2 and form a stable compound, Mg_2Cu . Mg_2Cu disproportionates during hydrogenation as described in Eq. 9.



Thus, the alloy Mg_2Cu has a theoretical hydrogen capacity of $\rho_m = 2.62$ wt% H, and $\Delta H_f = -70$ kJ/mol H_2 [37, 38].

A sample of Mg/ Mg_2Cu was prepared by arc-melting Mg–Cu (85.5:14.5) [38]. The sample was hydrogenated using two different methods, (a) ($p(\text{H}_2) = 6$ bar and $T = 325$ °C), and the low hydrogen pressure should facilitate the formation of MgH_2 – Mg_2Cu and (b), ($p(\text{H}_2) = 30$ bar and $T = 325$ °C) in order to facilitate the formation of MgH_2 – MgCu_2 . The in situ SR-PXD results

[39] confirmed that the reversible alloy formed upon dehydrogenation. The apparent activation energy for the dehydrogenation of air-exposed $\text{MgH}_2/\text{Mg}_2\text{Cu}$ and $\text{MgH}_2/\text{MgCu}_2$ sample was found to be $E_A \sim 108$ and ~ 160 kJ/mol, respectively [39]. Furthermore, substantially improved dehydrogenation kinetics of MgH_2 and resistance towards oxidation of Mg due to the presence of $\text{Mg}_2\text{Cu}/\text{MgCu}_2$ is observed. The apparent activation energy found for dehydrogenation of MgH_2 in $\text{MgH}_2/\text{Mg}_2\text{Cu}$ is in agreement with previous work [38]. The activation energies extracted for the air-exposed samples may be assumed to be maximum values, which may be relevant to know for practical applications. This work also illustrates that in situ synchrotron radiation powder X-ray diffraction (SR-PXD) is a useful technique for investigation of kinetic properties [40, 41]. These results indicate that the presence of either Mg_2Cu or MgCu_2 in MgH_2 has a pronounced positive effect on the dehydrogenation kinetics of air-exposed samples.

In addition to diffusion of hydrogen, hydrogen cycling requires solid-state diffusion of Mg, transforming it from the Mg-poor to the Mg-rich state of the alloy and vice versa. Solid-state diffusion, and hence the hydrogen sorption reaction in this system, is rather slow. Hence, one of the areas of recent study is the effect of reducing particle sizes. Supported nanocrystallites with an average size of 20 nm were prepared by initial deposition of Cu nanoparticles followed by Mg deposition and hydrogenation [42]. The temperature for hydrogen desorption was ~ 150 °C lower than for micron-sized material, and the kinetic performance was stable upon cycling. An activation energy for the hydrogen desorption of only 97 kJ/mol was found, clearly demonstrating the benefits of a reduction in particle size for the sorption kinetics, however at the expense of hydrogen storage capacity due to the carbon support.

1.3.3 Cobalt

The Mg–Co system contains only one intermetallic compound, a Laves-type MgCo_2 . However, sintering of the mixtures of the fine metal powders of Mg and Co at 450–500 °C and hydrogen pressure (90 bar), or reactive ball-milling of the stoichiometric 2:1 mixtures of Mg and Co under hydrogen gas leads to the formation of Mg_2CoH_5 .

Substitution of Fe in Mg_2FeH_6 by Co results in the formation of Mg_2CoH_5 with a smaller H/M ratio of 5/3 instead of 2.0, and with a much decreased thermal stability. Hydrogen desorption from Mg_2CoH_5 is a multistep process, which at 500 °C leads to the formation of MgCo and Mg [43]. This process is, however, reversible and allows the synthesis of Mg_2CoH_5 when the mixture MgCo + Mg is heated above 300 °C under a hydrogen pressure of 100 bar.

Hydrogenation of the MgCo_2 intermetallic alloy has been tried at similar high-pressure conditions to those applied to MgNi_2 . However, the metal sublattice becomes destabilized by Co which disproportionates to Mg_2CoH_5 and Co. The solid-solution-type ternary alloys $\text{MgNi}_{2-x}\text{Co}_x$ ($x = 0.25; 0.5, \text{ and } 0.75$) also are unstable compared with disproportionation into $\text{Mg}_2(\text{Ni},\text{Co})\text{H}_{5-x}$, even with the smallest content of Co at $x = 0.25$ (Antonov, Denys, Yartys, unpublished, 2015).

1.3.4 Titanium

Hydrogen storage behaviour of Mg nanoparticles (size range 100 nm to 1 μm) with metal-oxide core-shell morphology synthesized by inert gas condensation and decorated by titanium clusters via in situ vacuum deposition has been reported to improve only the kinetics [44]. Beside the alloying effect with transition metals, composite materials made of Mg with immiscible metals can also be prepared [36, 45]. Ponthieu et al. [46] investigated the Mg-Ti-H system focusing on MgH_2 - TiH_2 nanocomposites. They observed that this mixture leads to materials exhibiting very fast sorption kinetics. The samples were prepared by ball-milling of various mixtures of Mg and Ti under hydrogen pressure. In this way, nanocomposites were prepared in the range $x = 0$ to 0.5 for the system $(1-x)\text{MgH}_2-x\text{TiH}_2$. They consist of MgH_2 (with the coexistence of α - and γ -polymorphs) and ε - TiH_2 homogeneously distributed with crystallite sizes below 15 nm. A study of the sorption properties showed that only the magnesium hydride is reversible under moderate conditions ($T < 330$ °C, $p(\text{H}_2) < 1$ MPa), and the thermodynamics of the Mg/MgD_2 equilibrium is not affected. However, the presence of the titanium hydride leads to very fast hydrogen sorption kinetics for the magnesium system. Indeed, TiH_2 inclusions with particle sizes of 10 nm are found homogeneously distributed within the MgH_2 matrix, and a coherent coupling between titanium hydride inclusions and the Mg/MgD_2 matrix has been reported. This coupling is expected to enhance hydrogen mobility within the nanocomposite components as TiH_2 inclusions limit grain growth of both Mg and MgH_2 phases preserving short diffusion paths for hydrogen. Furthermore, TiH_2 is expected to favour the diffusivity of hydrogen through the existence of coherent coupling between TiH_2 and Mg/MgH_2 . Though TiH_2 does not influence the Mg/MgD_2 thermodynamics, it provides fast sorption kinetics, allowing the nanocomposites to absorb large amounts of hydrogen at room temperature. These kinetic properties are attributed to the limited grain growth of Mg and MgD_2 phases, the coherent coupling between TiH_2 and Mg/MgH_2 , and the fast H-diffusion through sub-stoichiometric $\text{MgD}_{2-\eta}$ and $\text{TiD}_{2-\eta}$ phases.

1.3.5 Palladium

The Mg-Pd phase diagram is rather complex and comprises several intermetallic phases. The Mg_6Pd phases have attracted most interest for hydrogen storage, as it is the lightest and least costly intermetallic. Mg-Pd composite nanoparticles were synthesized by inert gas condensation of Mg vapours followed by vacuum evaporation of Pd clusters. Formation of the Mg_6Pd intermetallic phase takes place upon vacuum annealing, resulting in $\text{Mg}/\text{Mg}_6\text{Pd}$, which transforms to different Mg-Pd intermetallic compounds upon hydrogen absorption, depending on temperature and pressure [47].

Mg_6Pd nanoparticles of 4 nm were obtained by infiltration of Mg on previously formed Pd nanoparticles dispersed into the pores of porous carbon [48]. Mg infiltration resulted in the in situ formation of intermetallic Mg_6Pd nanoparticles. From the EXAFS-based structural analysis, it was demonstrated that the crystal structure of the nanoparticles is different than bulk Mg_6Pd . The nanoparticles exhibit a simpler crystallographic arrangement and a higher atomic disorder. As for the structural properties, thermodynamic and kinetic sorption properties also show different behaviours than for the bulk material. A change in the plateau pressure (Fig. 6) indicating thermodynamic destabilization of the hydride phase has been reported. In addition, faster kinetics were observed for the Mg_6Pd nanoparticles (Fig. 7) that remain stable for at least 10 sorption cycles though the particle size increased from 4 nm in the as-synthesized compound to 10 nm after hydrogenation. This modification of the sorption properties is related to the small particle size, as well as the difference in the crystal structure compared to that of bulk Mg_6Pd .

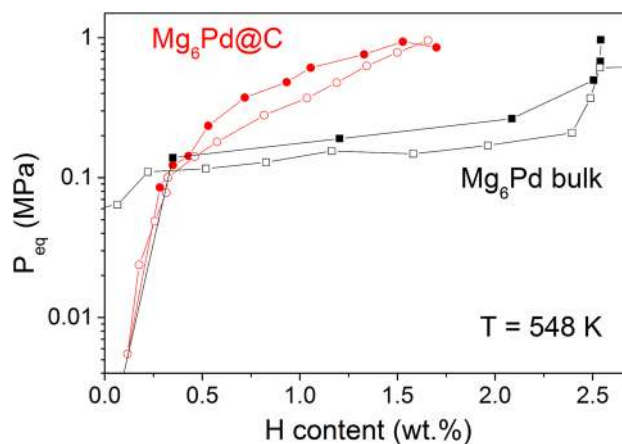


Fig. 6 Hydrogen sorption isotherms at 275 °C for the bulk (black line) and nanoconfined (red line) Mg_6Pd . Full and empty symbols stand for absorption and desorption isotherm curves, respectively [48]

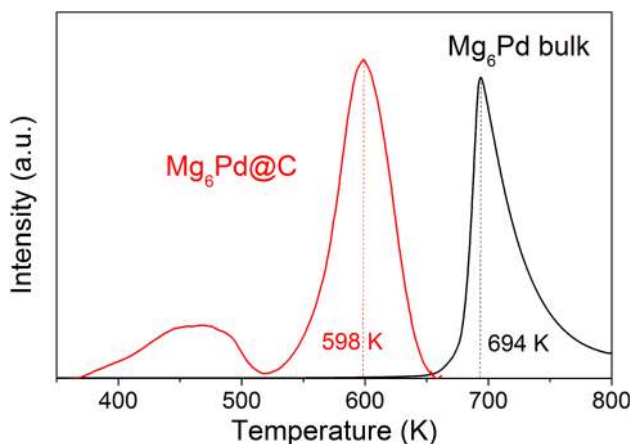
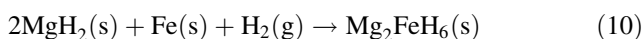


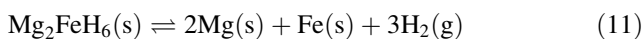
Fig. 7 Thermal hydrogen desorption mass spectra of hydrogenated bulk (black line) and nanoconfined (red line) Mg_6Pd ($m/e = 2$, heating rate $5^\circ\text{C}/\text{min}$) [48]

1.3.6 Iron

Magnesium iron hydride is known to have one of the highest volumetric hydrogen density of $\rho_v = 150 \text{ g H}_2/\text{L}$, moderate gravimetric storage density $\rho_m = 5.47 \text{ wt\% H}$ and can be prepared from inexpensive chemicals [49–51]. The Mg_2Fe alloy is stabilized by hydrogen, i.e. Mg_2FeH_6 forms in a reaction between magnesium hydride and iron at $T > T_{\text{dec}}(\text{MgH}_2)$. The reaction (Eq. 10) for a sample of $\text{MgH}_2\text{--Fe}$ (2:1) in the temperature range $380\text{--}470^\circ\text{C}$, $p(\text{H}_2) = 100 \text{ bar}$, was studied using in situ SR-PXD. The hydrogen pressure stabilizes the MgH_2 and facilitates the reaction.



Mg_2FeH_6 was cooled to RT where it is stable and then heated in argon ($p(\text{Ar}) = 1 \text{ bar}$). A series of in situ SR-PXD patterns revealed that Mg_2FeH_6 apparently decomposes directly to the metals according to reaction (Eq. 11) in agreement with previous investigations and the fact that $T_{\text{dec}}(\text{Mg}_2\text{FeH}_6) > T_{\text{dec}}(\text{MgH}_2)$, $\Delta H_{\text{dec}}(\text{Mg}_2\text{FeH}_6) = 87 \pm 3 \text{ kJ/mol H}_2$ [52].



1.3.7 Zinc

Mg--Zn alloys have been investigated for hydrogen storage but have not been found to improve the storage properties of Mg [52]. *Ex situ* X-ray diffraction has been used to show that the Zn forms an intermetallic alloy with Mg, which upon absorption of hydrogen either remains unaffected [52] or forms a higher Zn content intermetallic alloying more Mg to form a hydride [53, 54]. However, it has also been shown by in situ neutron diffraction that a Zn-containing

liquid phase forms at the temperatures typically used for hydrogenation [55]. No Zn hydride or Mg--Zn ternary hydride has been observed.

1.4 Mg-containing quasicrystals

Quasicrystals (QCs) are materials with long-range order but which lack three-dimensional translational periodicity. The first of these structures discovered was a rapidly solidified Al--Mn alloy [56]. Over a hundred binary and ternary QC intermetallic systems have been discovered; half of these are metastable and require rapid solidification production techniques, such as splat cooling or melt spinning [57]. The initial QC systems were mostly Al-based; however, Mg-containing QCs in the Mg--Zn--(Y, RE) system were reported by Luo et al. [58]. QC structures present the opportunity to develop new hydride systems, with unusual physical and mechanical properties [59] and high H/M ratios because there are more interstitial sites for hydrogen compared to conventional hydrides. A limited number of studies have explored the hydrogen storage properties of QC systems, most of which focus on Ti-based QCs, for example Ti--Zr--Ni and Ti--Hf--Ni . These achieved relatively high hydrogen storage capacities ($\text{H/M} = 1.6$), but the recovery of the QC phase was difficult, due to the formation of ZrH_2 or TiH_2 and Ti_2Ni alloy after one (de)hydrogenation cycle [60, 61]. Sahlberg and Andersson [62] initially investigated the hydrogenation properties of a cubic $\text{Mg}_3\text{Y}_2\text{Zn}_3$ ternary alloy with limited success. It only hydrogenated above 400°C and had a low hydrogen storage capacity (0.3 wt%).

More recently, Luo et al. [63] presented a study on the hydrogenation properties of a Zn--Mg--Y quasicrystal and its ternary alloys. The approximate stoichiometry of the stable Zn--Mg--Y icosahedral QC (i-phase) was confirmed to be $\text{Zn}_{60}\text{Mg}_{30}\text{Y}_{10}$. Three nominal compositions were prepared: ZMY-1, $\text{Zn}_{50}\text{Mg}_{42}\text{Y}_8$ by gas atomization in an argon atmosphere; ZMY-2, $\text{Zn}_{60}\text{Mg}_{30}\text{Y}_{10}$ by induction melting; and ZMY-3, $\text{Zn}_{60}\text{Mg}_{30}\text{Y}_{10}$ by gas atomization followed by annealing at 585°C . The as-prepared samples were ball-milled under 1 bar Ar for 2 h. A quasicrystal i-phase was observed in all three as-prepared Zn--Mg--Y alloy samples, (Fig. 8). Despite using different preparation methods and initial nominal compositions, ZMY-1 and ZMY2 showed similar XRD patterns consisting of two major phases, i-phase and a H-phase (hexagonal $(\text{Zn,Mg})_5\text{Y}$ alloy). Unlike the other two samples, ZMY-3 exhibited peaks only associated with the i-phase.

The SEM image of the as-prepared ZMY-1 sample (Fig. 9a) shows that spherical particles of sizes smaller than $200 \mu\text{m}$ were formed through gas atomization, with a distinctive structure on the surface, while cross-sectional SEM backscattered electron (BSE) images of ZMY-1 and

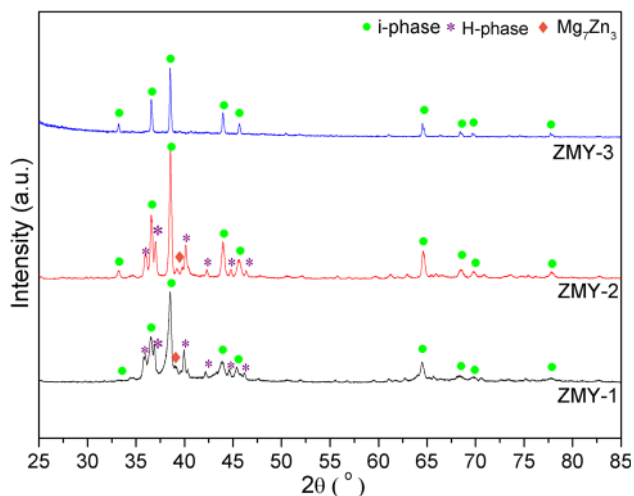


Fig. 8 X-ray diffraction patterns of as-prepared Zn–Mg–Y samples. ZMY-1 and ZMY-2 consisted of three phases including a QC i-phase, H-phase, and Mg_7Zn_3 , while the ZMY-3 sample consisted of a single i-phase [50]

ZMY-2 (Fig. 9b, c) indicated the presence of i-phase and H-phase in both samples, with different microstructures. ZMY-1 was formed of a petal-like i-phase surrounded by small white dots (ca. 1 μm) from the H-phase, while ZMY-2 consisted of dendritic H-phase structures located in the middle of the i-phase. The i-phase dominated ZMY-3, accounting for >95 % of the volume fraction based on cross-sectional BSE imaging.

The annealed Zn–Mg–Y QC sample (ZMY-3) had a 0.3 wt% hydrogen storage capacity and a high DSC decomposition temperature (503 $^{\circ}C$), while higher hydrogen storage capacity (0.9 wt%) and lower decomposition temperature (445 $^{\circ}C$) were achieved with ZMY-1, which had a greater H-phase contribution. The H-phase contains a greater proportion of Y that may cause the expansion of the unit cell and thus facilitate the hosting of more hydrogen atoms, as in ZMY-1. In addition, the lower decomposition temperature may be attributed to a smaller i-phase grain resulting in faster kinetics. TGA results showed that ZMY-1, ZMY-2, and ZMY-3 released 1.0 ± 0.1 , 0.3 ± 0.1 , and 0.4 ± 0.1 wt% of hydrogen, respectively, which was in close agreement with the PCI curves. A hydrogenation plateau (of ca. 3.5 bar) was observed on its PCI curve at 300 $^{\circ}C$ which suggests an improvement on the thermodynamics of MgH_2 (1.4 bar at 300 $^{\circ}C$). Further work is required to investigate the (de)hydrogenation reaction mechanism and speed up the reaction kinetics.

1.5 RE–Mg–Ni hydrides (RE = La, Pr, Nd)

Despite significant differences in chemistry between the rare earth metals (RE) and magnesium, Mg forms extensive solid solutions in the $RENi_3$ intermetallic alloys,

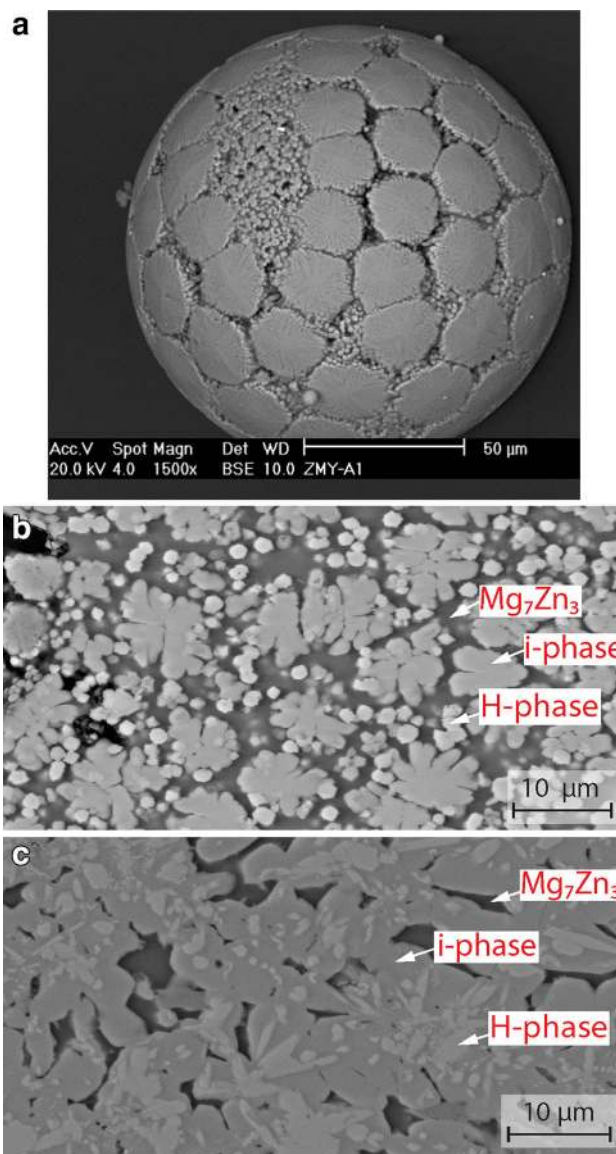


Fig. 9 SEM backscattered electron (BSE) images of **a** surface as-prepared ZMY-1, **b** cross-sectional ZMY-1, and **c** cross-sectional ZMY-2 [50]

crystallizing with a $PuNi_3$ -type trigonal structure. Up to 67 % of RE atoms can be replaced by Mg to form $REMg_2Ni_9$ intermetallic compound. The $RENi_3$ crystal structures are formed by a stacking of the $RENi_5$ (*Haucke* $CaCu_5$ type) and $RENi_2$ (*Laves* type) slabs along the trigonal $00z$ axis ($RENi_5 + 2MgNi_2 = REMg_2Ni_9$). The substitution $Mg \rightarrow RE$ takes place within the Laves-type slabs only leaving $RENi_5$ layers unmodified ($RENi_5 + 2MgNi_2 = REMg_2Ni_9$). In fact, a small yet significant replacement of RE by Mg (5 %) was observed in $La_{0.91}Mg_{2.09}Ni_9$ within the AB_5 slabs leading to the formation of the over-stoichiometric compositions $RE_{1-x}Mg_{2+x}Ni_9$ crystallizing with $PuNi_3$ -type structure.

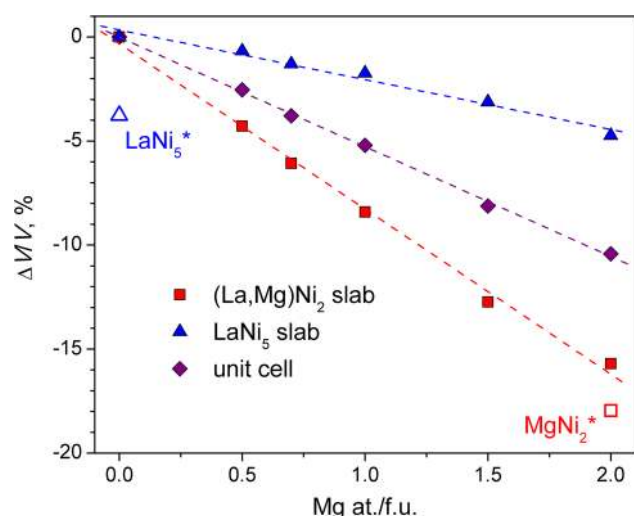


Fig. 10 Relative changes in the volumes of the unit cells and constituent fragments of the $\text{La}_{3-x}\text{Mg}_x\text{Ni}_9$ structures during the $\text{Mg} \rightarrow \text{La}$ substitution. The data for the individual LaNi_5 and MgNi_2 compounds are given as a reference

A gradual increase in Mg content in $\text{RE}_{3-x}\text{Mg}_x\text{Ni}_9$ is accompanied by a linear decrease in the volumes of the unit cells (Fig. 10). Interestingly, a substantial contraction takes place not only for the $(\text{RE},\text{Mg})_2\text{Ni}_4$ slabs, but also for Mg-free CaCu_5 -type RENi_5 slabs [64].

Magnesium significantly affects the bonding mechanism of metal–hydrogen interactions studied in detail for La_2MgNi_9 -based hydride [65]. A prominent and the most important feature of the structure of $\text{La}_2\text{MgNi}_9\text{D}_{13}$ is in the local ordering of the hydrogen sublattice built by stacking of the MgH_6 octahedra and NiH_4 tetrahedra (Fig. 11).

Substitution of the largest (in size) atom of the rare earth metals—lanthanum—by smaller atoms like Pr or Nd leads to the contraction of the volumes of the unit cells of $(\text{La},\text{Pr},\text{Nd})_2\text{MgNi}_9$, reaching 2.6 % for Nd_2MgNi_9 [66]. The hydrogen storage capacity of the alloys remains unchanged, 12–13 at. $\text{H}/\text{f.u.}(\text{La},\text{Pr},\text{Nd})_2\text{MgNi}_9$. However, shrinking of the lattice quite significantly affects the thermodynamic stability of the formed hydrides. As evident from the room-temperature isotherms (Fig. 12), equilibrium pressures of both hydrogen absorption and desorption in the $\text{Nd}_2\text{MgNi}_9\text{-H}_2$ system are an order of magnitude higher than in the $\text{La}_2\text{MgNi}_9\text{-H}_2$ system changing from <0.1 bar for the La_2MgNi_9 -based hydride to >1 bar for $\text{Nd}_2\text{MgNi}_9\text{H}_{12}$.

The properties of $\text{RE}_{3-x}\text{Mg}_x\text{Ni}_9$ -based hydrides dramatically change when the content of magnesium extends to the maximum solubility limit, close to two atoms of Mg/f.u. for $\text{RE}_{3-x}\text{Mg}_x\text{Ni}_9$. In situ neutron powder diffraction studies of two deuterides $\text{La}_{1.09}\text{Mg}_{1.91}\text{Ni}_9\text{D}_{9.5}$ and $\text{La}_{0.91}\text{Mg}_{2.09}\text{Ni}_9\text{D}_{9.4}$ performed at deuterium pressures reaching 918 bar D_2 showed that the hydrogenation properties of Mg-rich

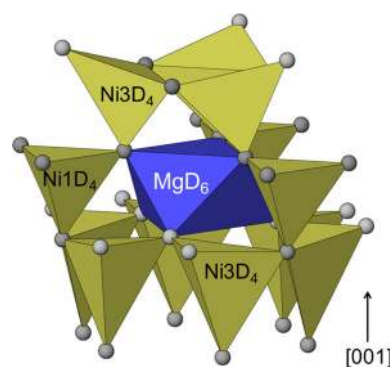


Fig. 11 Hydrogen sublattice for the $\text{La}_2\text{MgNi}_9\text{D}_{13}$ structure. The sublattice is formed by the stacking of MgD_6 octahedra and NiD_4 tetrahedra. Such stacking gives an irregular, buckled framework

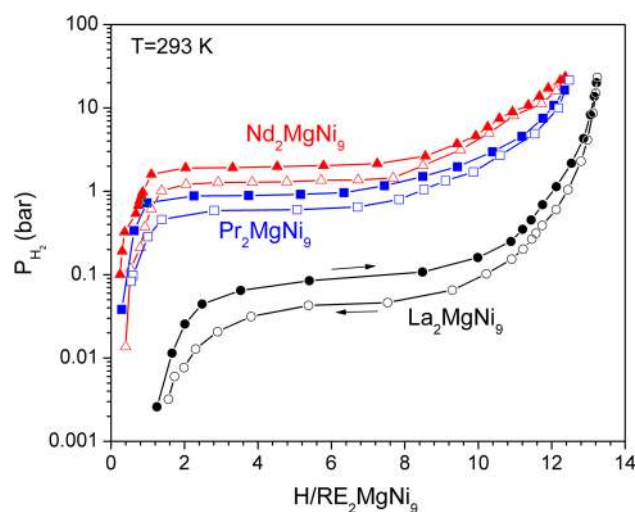


Fig. 12 PCT diagrams for $\text{Nd}_2\text{MgNi}_9\text{-H}_2$, $\text{Pr}_2\text{MgNi}_9\text{-H}_2$, and $\text{La}_2\text{MgNi}_9\text{-H}_2$ systems

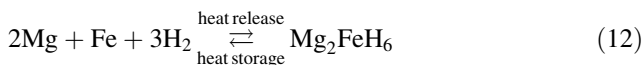
compounds are principally different from those for LaNi_3 [67]. LaNi_5 -assisted hydrogenation of MgNi_2 in the hybrid structure of LaMg_2Ni_9 takes place. In the deuterides, the D atoms are accommodated in both Laves- and CaCu_5 -type slabs. The overall chemical compositions can be presented as $\text{LaNi}_5\text{H}_{5.6/5.0} + 2 * \text{MgNi}_2\text{H}_{1.95/2.2}$ showing that the hydrogenation of the MgNi_2 slab proceeds at mild H_2/D_2 pressure of just 20 bar. A partial filling by D of the four types of the tetrahedral interstices in the MgNi_2 slab takes place, including $[\text{MgNi}_3]$ and $[\text{Mg}_2\text{Ni}_2]$ tetrahedra. Magnesium causes a significant destabilization of the hydrides; $\text{La}_{1.09}\text{Mg}_{1.91}\text{Ni}_9$ reversibly forms hydrides with $\Delta H_{\text{des}} = 24.0 \text{ kJ/mol H}_2$ (as compared to $\Delta H_{\text{des}} = 35.9 \text{ kJ/mol H}_2$ for La_2MgNi_9 [66]) and an equilibrium pressure of H_2 desorption of 18 bar at 20 °C (0.05 bar at 20 °C for La_2MgNi_9 [65]). However, magnesium also introduces a pronounced hysteresis of H_2 absorption and desorption, ~100 bar. The latter is probably caused by a huge

difference in the dimensions of the Ni net in the individual crystal lattices of MgNi_2 and LaNi_5 .

1.6 Magnesium compounds for high-temperature energy storage

Thermochemical gas–solid reactions are suitable as long-term or short-term heat storage systems. Important for short-term heat storage systems is good kinetics of the absorption and desorption of the gaseous compound combined with good heat conductivity of the reaction bed. After separation of both compounds during the decomposition process, all of this energy is trapped in the system and can be used at any time without energy losses (long-term storage). Reversible Mg-based metal hydride systems show a rather high range of energy densities (62–77 kJ/mol H_2 ; see Table 1) making their use convenient in thermochemical heat storage systems, even though the values 62–77 kJ/mol H_2 are significantly lower as compared to the highest observed values for the metal hydrides, $\text{YH}_{1.8}$ (220 kJ/mol H_2), $\text{ZrH}_{1.6}$ (212 kJ/mol H_2) and CaH_2 (207.7 kJ/mol H_2) [68].

While research in past years has been focused on the pure Mg/ MgH_2 system, which can be used for temperatures up to 400 °C in solar power parabolic trough systems, new developments now focus on the 2 Mg + Fe/ Mg_2FeH_6 system. This material can be used at temperatures up to 550 °C as a possible heat storage material for the solar tower power plants and shows excellent stability over hundreds of hydrogenation and dehydrogenation cycles (Eq. 12).



Current research is focused on the identification of cost-effective materials undergoing hydrogenation–dehydrogenation reactions (heat storage–heat release) with a high degree of reversibility upon multiple cycles and fast and controllable kinetics [69]. A wide range of temperatures with different Mg-based metal hydrides between 400 and 600 °C can be covered.

1.7 The HDDR processes in the Mg-based alloys (LaMg_{12} , $\text{LaMg}_{11}\text{Ni}$)

The hydrogenation–disproportionation–desorption–recombination (HDDR) process includes two stages of hydrogen absorption, normally at relatively lower and higher temperatures promoting, respectively, the formation of interstitial hydrides with expanded cells and the disproportionation of the metallic matrix of this hydride accompanied by the formation of binary hydrides and other phases with reduced (zero) content of the hydride-forming element, e.g. the products of disproportionation.

The high-temperature desorption of hydrogen is accompanied by the recombination of the source compound but already with sub-micrometre grain sizes. For the magnesium-rich compounds of rare earth metals, because of a very large enthalpy of formation of both MgH_2 (−74 kJ/mol H_2) and rare earth metals (−208 kJ/mol H_2 for LaH_2), the formation of the interstitial-type hydrides becomes thermodynamically unfavourable as compared to the formation of the hydrides of Mg and rare earth metals. However, even though the decomposition of the rare earth hydrides needs application of extremely high temperatures, more than 800 °C (in vacuum) for LaH_2 , it becomes destabilized by magnesium metal formed during hydrogen desorption from MgH_2 . This makes possible a recombination of the intermetallics of rare earths and magnesium below 450 °C. The latter temperature is 400 °C lower than the temperature required to decompose individual LaH_2 .

In the case of LaMg_{12} , hydrogen absorption resulted in a two-step disproportionation process: $\text{LaMg}_{12} + \text{H}_2 \rightarrow \text{LaH}_3 + \text{Mg} \rightarrow \text{LaH}_3 + \text{MgH}_2$ [33]. It is interesting that instead of immediate formation of MgH_2 , the magnesium metal was formed first, before interacting with hydrogen to yield a magnesium dihydride.

A decrease in the grain size of the initial alloy was achieved by applying a rapid solidification (RS) process, and this was found to assist in improving the hydrogenation kinetics. It is interesting to note that ribbons of the RS samples retained their initial shapes after the hydrogenation despite the fact that formation of LaH_3 and MgH_2 hydrides is accompanied by a significant volume expansion.

Hydrogen thermal desorption in vacuum occurred in different ways for the alloys solidified at different quenching rates. A major peak of hydrogen evolution was located at ~370 °C; however, for the alloys synthesized by rapid solidification and having the smallest grain size, an extra desorption event was observed at 415 °C (Fig. 13). SR XRD study showed that this extra peak is associated with Mg-assisted low-temperature hydrogen desorption from LaH_2 proceeding below 450 °C and leading to a recombination process to form the initial intermetallic alloy LaMg_{12} .

The chemical equations taking place in these two processes can be described as follows:

1. Desorption without recombination (RS samples prepared at low solidification rate and as-cast samples)

$$\text{MgH}_2 + \text{LaH}_3 \rightarrow \text{Mg} + \text{LaH}_2 + 3/2\text{H}_2$$
2. Desorption followed by recombination of LaMg_{12} (RS samples prepared at high solidification rate)

$$12\text{MgH}_2 + \text{LaH}_3 \rightarrow 12\text{Mg} + \text{LaH}_2 + 25/2\text{H}_2$$

$$\rightarrow \text{LaMg}_{12} + \text{H}_2$$

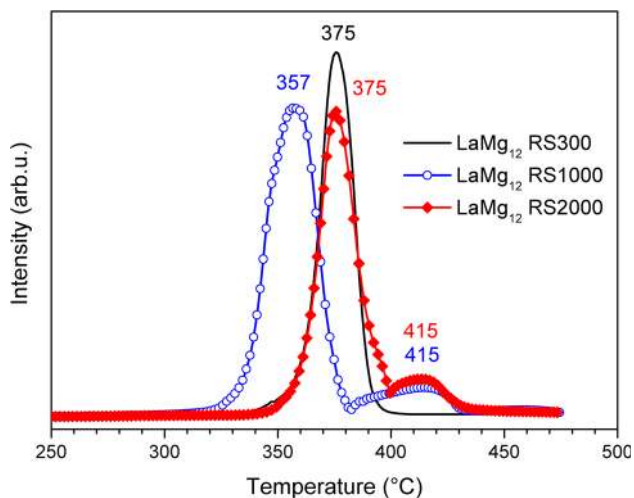


Fig. 13 Hydrogen thermal desorption mass spectra of the hydrogenated RS alloys measured in vacuum

SEM studies revealed significant differences between the samples after completion of the thermal desorption of hydrogen. Samples for which the recombination stage was observed were found to have extremely porous morphology (pore sizes 0.5–2 μm ; see Fig. 14). Such dramatic microstructural changes can be attributed to the recombination of the LaMg_{12-x} intermetallic during H desorption and associated with volume shrinkage during the

$\text{Mg} + \text{LaH}_2 \rightarrow \text{LaMg}_{12-x} + \text{H}_2$ transformation. No such transformation took place in the RS samples prepared at low solidification rate and the as-cast samples, which is attributed to their coarse initial microstructures. These observations show that fine nanostructuring of the material leads to a complete recombination process and to the enhancement of hydrogen exchange.

From comparison of the data for LaMg_{12} [33] with the results for the rapidly solidified $\text{LaMg}_{11}\text{Ni}$ alloy where 1/12 of Mg was substituted by Ni [34, 35], it has been concluded that Ni substitution in combination with rapid solidification significantly improves the hydrogenation–desorption properties of the alloy leading to a dramatic increase in the rates of hydrogenation–dehydrogenation processes as a result of the nanostructuring of the samples and because of the catalytic influence of the formed Mg_2Ni intermetallics. On hydrogen desorption, the presence of mobile hydrogen in the metal lattice allows a low-temperature diffusion of both lanthanum and magnesium to proceed. Because of the thermodynamic advantage of the formation of La–Mg intermetallics compared to the mixture of Mg metal and lanthanum dihydride, this causes a recombination reaction to proceed below 450 $^\circ\text{C}$, 400 $^\circ\text{C}$ lower than the decomposition temperature of LaH_2 , to sequentially form LaMg_{12-x} , and later, $\text{La}_2\text{Mg}_{17}$ intermetallics (Fig. 15).

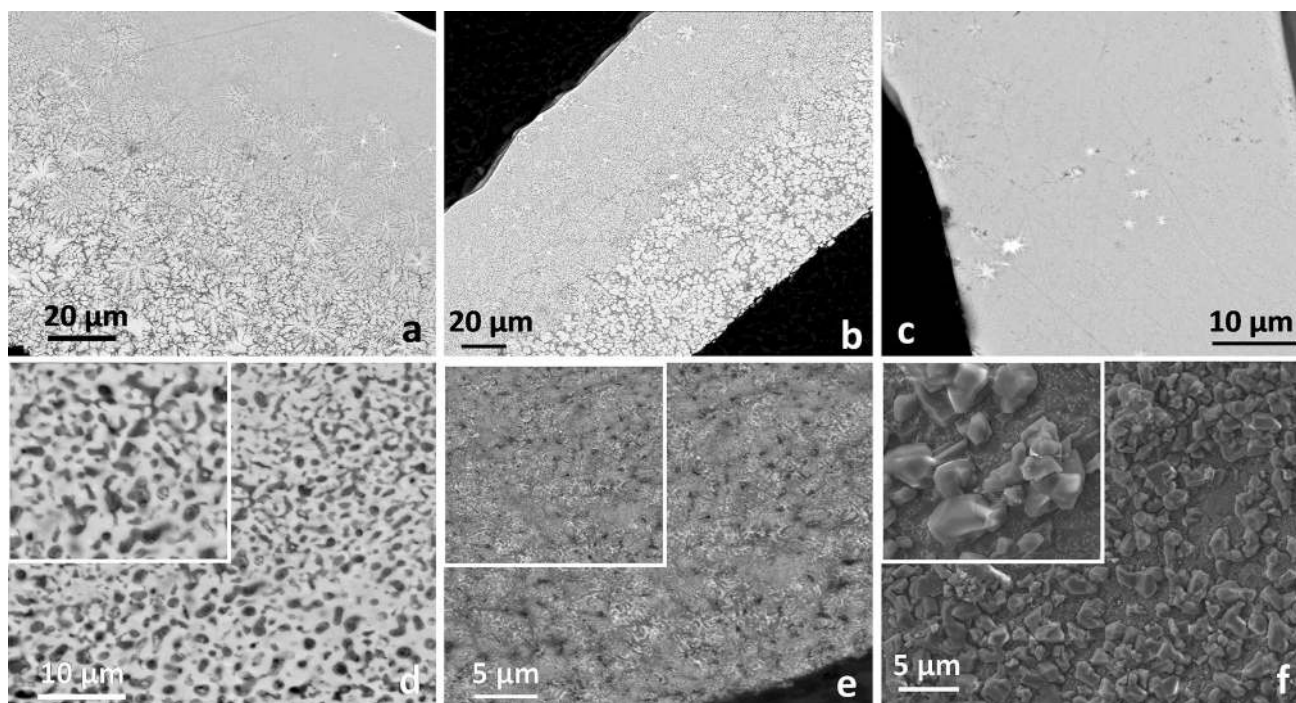
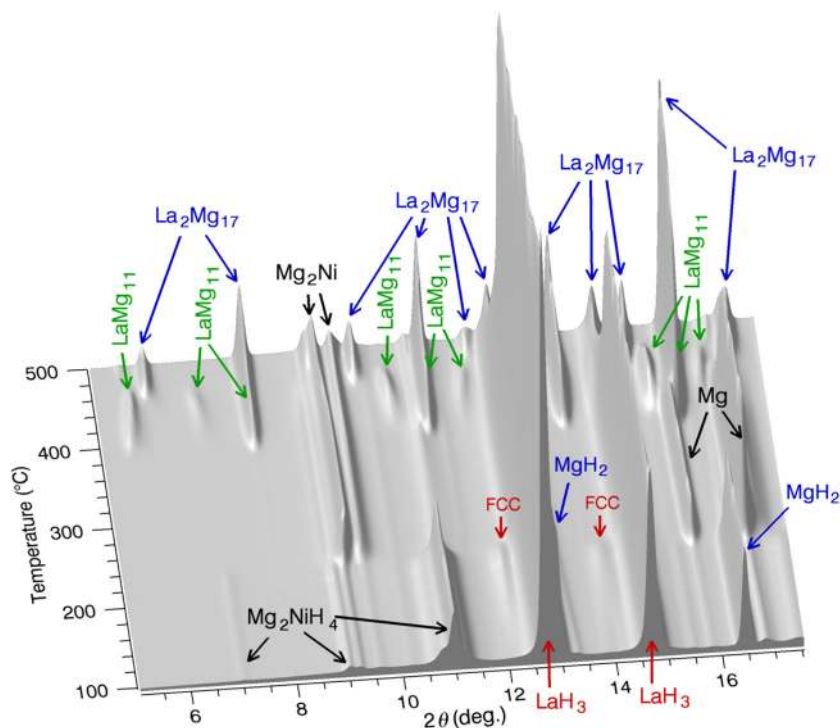


Fig. 14 Backscattered SEM images of the RS LaMg_{12} samples (a RS300; b RS1000; c RS2000) and RS2000 sample at different stages of hydrogen processing (d after TDS from the hydride; e, after

five hydrogen absorption–desorption cycles; f hydrogenated sample). For the inserted magnified square areas, the sides are 5 μm

Fig. 15 Evolution of the in situ SR XRD pattern from the hydrogenated $\text{LaMg}_{11}\text{Ni}$ alloy during hydrogen vacuum thermal desorption in the temperature range 100–500 °C (heating rate 2 °C/min; SNBL BM01A; $\lambda = 0.72085 \text{ \AA}$). Peaks marked FCC correspond to a LaHO oxyhydride



Ribbons of the RS samples retained their initial shapes despite the fact that formation of LaH_3 and MgH_2 hydrides is accompanied by a significant volume expansion.

2 First-principle study on Mg-based hydrides

Between interstitial metal hydrides, such as LaNi_5H_6 , and ionic complexes, such as Mg_2NiH_4 , a large family of (La,Mg)-Ni hydrides exists, exhibiting intermediate electronic properties. The host intermetallics belong to the $(\text{La,Mg})\text{Ni}_y$ family, with $y = (5n + 4)/(n + 2)$. It has been shown [70] that such intermetallics are stabilized by the stacking along the c -axis of $n * [\text{LaNi}_5] + m * [\text{LaMgNi}_4]$ layers of *Haucke* and *Laves* phases, respectively, with Mg atoms occupying only half La sites of the latter. In this context, a systematic investigation of the electronic properties of the $(\text{La,Mg})_2\text{Ni}_7\text{H}_x$ hydrides has been recently done [71]. To understand the preferential interstitial H sites, a systematic comparison of 13 different sites showed that both geometrical and chemical factors govern the stability of the hydrides of the RE–Mg–Ni family. It has been shown that the calculated site preferences are in agreement with the experimental data, for which H occupies $[\text{La}_2\text{Ni}_4]$ slab in La_2Ni_7 compound mainly for geometrical reasons, whereas H goes in both $[(\text{La,Mg})_2\text{Ni}_4]$ and $[\text{LaNi}_5]$ slabs for the Mg-substituted compound driven by both geometrical and chemical factors. The $\text{La}_{1.5}\text{Mg}_{0.5}\text{Ni}_7$ hydrides show electronic charge transfer from La

and Mg to H. Depending on the H site environment, the Bader charge analysis gives a value of about $-0.31e$ on H, which classifies these hydrides as conventional metallic ones, such as LaNi_5H_x .

Another interesting study on Mg-based hydrides has been recently published on the trihydride MgNi_2H_3 [36, 72]. The DFT calculations showed the formation of an electronic structure around -10 to -6 eV caused by the chemical bonds of hydrogen and its $1s$ states mainly via interaction with the Ni $3d$ states. The bonding mechanism is dominated by the formation of covalent bonds between Ni and H and a charge transfer from Mg to the two different H atoms which leads to a significant degree of ionic bonding between Mg ($+1.59e$) and H ($-0.55e$, $-0.31e$). The calculated enthalpy of formation of MgNi_2H_3 is approximately -30 kJ/mol H_2 , which is consistent with the stability of a hydride at normal conditions. Moreover, the analysis of calculated phonon dispersion curves has confirmed that the structure is mechanically stable in *Cmca* symmetry (Fig. 16), the most stable one among all considered alternatives. In addition, the thermodynamic properties of MgNi_2H_3 with temperature and volume dependence have been estimated in the frame of the quasiharmonic approximation.

The variety of chemical bondings within Mg-based hydrides is illustrated in Fig. 17, showing the electron localization function (ELF) representations for several compounds. The probability function ranges between 0 (no probability) and 1 (perfect localization) for the valence

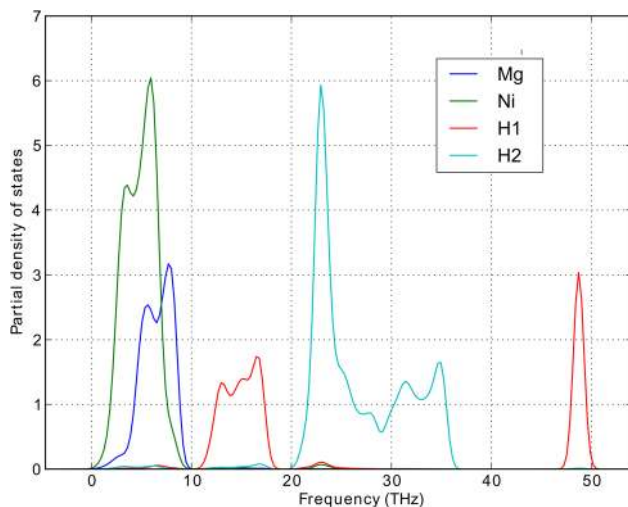
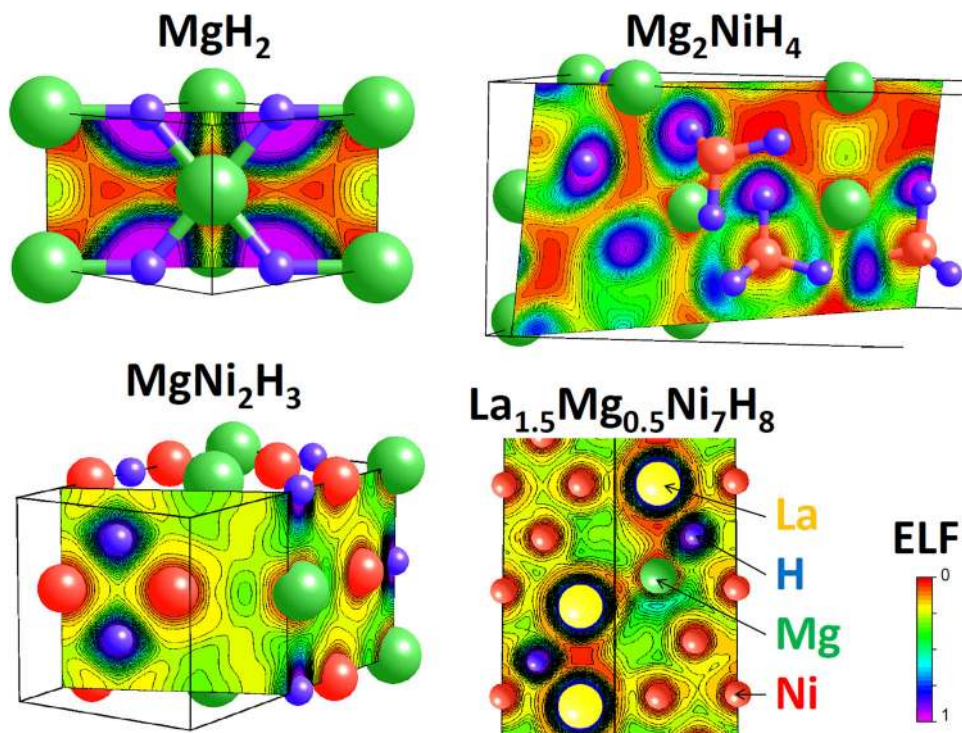


Fig. 16 Partial phonon density of state (DOS) of MgNi_2H_3 in the $Cmca$ space group

electrons, 0.5 indicating probability similar to electron gas. Whereas MgH_2 and Mg_2NiH_4 show isolated anions around H atoms with a partial negative charge, and tetrahedral $[\text{NiH}_4]^{2-}$ complex, respectively, the hydrides $\text{La}_{1.5}\text{Mg}_{0.5}\text{Ni}_7\text{H}_x$ and MgNi_2H_3 exhibit a non-null ELF region (>0.25) between Mg and H. This behaviour fully shows that the partial covalent interaction between Mg and H is typical for a variety of magnesium-containing hydrides.

Fig. 17 Electron localization function (ELF) images of selected planes containing Mg and H atoms into MgH_2 ($P4_2/mmm$), Mg_2NiH_4 ($C12$), MgNi_2H_3 ($Cmca$), and $\text{La}_{1.5}\text{Mg}_{0.5}\text{Ni}_7\text{H}_8$ ($P6_3/mmc$)



3 Concluding remarks

Magnesium-based compounds continue to be the subject of intensive research for hydrogen storage, due to their light weight and inexpensive availability of magnesium. Practical limitations on the application for the pure metal, such as slow kinetics and high temperatures of desorption, require the development of compound materials to overcome these limitations. While improvements in kinetics have been achieved with nanostructuring processes, such as ball-milling, rapid solidification and other processes that introduce defects, and combination with relatively small amounts (<10 wt%) of additives [8], improvements in the thermodynamics are necessary to substantially reduce dehydrogenation temperatures. Alloys and intermetallic compounds of magnesium provide a way of reducing the enthalpy of the reaction compared to the pure metal hydride.

A large number of materials, mostly metals, have been used to form magnesium compounds and the thermodynamics of their interaction with hydrogen has been characterized. In many cases, the new hydrogenated compounds have reduced enthalpies; however, problems such as slower kinetics, instability, and disproportionation upon hydrogen cycling often arise. Sometimes the preparation process introduces metastable phases that, although beneficial to the interaction with hydrogen, are lost after

the initial hydrogen cycling. In addition, the introduction of another material to the magnesium typically results in a reduction in hydrogen capacity.

Binary compounds of magnesium have been investigated quite thoroughly, and it may be that the feasible alloys for effective, low-temperature hydrogen storage materials have been exhausted. Ternary and higher alloys may offer new possibilities in this area.

Finally, a new area of use of the Mg-based hydrogenated compounds appears to be heat storage. Here, for the entire range of temperatures, future research will include the identification of the most promising candidates together with the synthesis and the full thermodynamic/thermophysical and kinetics characterization [73]. Moreover, hydrides working at relatively low equilibrium pressure (between 1 and 50 bar) and at a certain selected temperature will be preferred in order to minimize the complexity and the cost of the thermal energy storage system.

The present special issue contains two other closely related papers which could be of interest for the readers entitled “Review of magnesium hydride based materials: development and optimisation” [74] and “Integrated with FC H storage systems utilising magnesium hydride: experimental Studies and modelling” [75].

Acknowledgments This work is a part of the activities within IEA Task 32 Hydrogen-based Energy Storage. We are grateful for the operating agent Dr. Michael Hirscher and all the experts from the Task 32 for the fruitful collaboration.

References

- M.B. Ley, L.H. Jepsen, Y.-S. Lee, Y.W. Cho, J.M. Bellosta von Colbe, M. Dornheim, M. Rokni, J.O. Jensen, M. Sloth, Y. Filinchuk, J.E. Jørgensen, F. Besenbacher, T.R. Jensen, Complex hydrides for hydrogen storage—new perspectives. *Mater. Today* **17**(3), 122–128 (2014)
- U. Eberle, M. Felderhoff, F. Schüth, Chemical and physical solutions for hydrogen storage. *Angew. Chem. Int. Ed.* **48**(36), 6608–6630 (2009)
- M. Dornheim, S. Doppiu, G. Barkhordarian, U. Boesenberg, T. Klassen, O. Gutfleisch, R. Bormann, Hydrogen storage in magnesium-based hydrides and hydride composites. *Scr. Mater.* **56**(10), 841–846 (2007)
- A. Zaluska, L. Zaluski, J.O. Ström-Olsen, Nanocrystalline magnesium for hydrogen storage. *J. Alloys Compd.* **288**(1–2), 217–225 (1999)
- J. Huot, G. Liang, R. Schulz, Mechanically alloyed metal hydride systems. *Appl. Phys. A Mater. Sci. Process.* **72**(2), 187–195 (2001)
- K. Alsabawi, T.A. Webb, E.M. Gray, C.J. Webb, Effect of C₆₀ Additive on Magnesium Hydride for Hydrogen Storage. *Int. J. Hydrog. Energy* **40**(33), 10508–10515 (2015)
- S. Bouaricha, J.P. Dodelet, D. Guay, J. Huot, R. Schulz, Study of the activation process of Mg-based hydrogen storage materials modified by graphite and other carbonaceous compounds. *J. Mater. Res.* **16**(10), 2893–2905 (2011)
- C.J. Webb, A review of catalyst-enhanced magnesium hydride as a hydrogen storage material. *J. Phys. Chem. Solids* **84**, 96–106 (2015)
- M. Paskevicius, D.A. Sheppard, K. Williamson, C.E. Buckley, Metal hydride thermal heat storage prototype for concentrating solar thermal power. *Energy* **88**, 469–477 (2015)
- A. Reiser, B. Bogdanovic, K. Schlichte, The application of Mg-based metal-hydrides as heat energy storage systems. *Int. J. Hydrog. Energy* **25**(5), 425–430 (2000)
- D.A. Sheppard, M. Paskevicius, C.E. Buckley, Thermodynamics of hydrogen desorption from NaMgH₃ and its application as a solar heat storage medium. *Chem. Mater.* **23**(19), 4298–4300 (2011)
- G.S. Walker, Multicomponent hydrogen storage systems, in *Solid-state Hydrogen Storage*, ed. by G.S. Walker (Woodhead Publishing Ltd, Cambridge, 2008), pp. 478–499
- J.J. Vajo, F. Mertens, C.C. Ahn, R.C. Bowman, B. Fultz, Altering hydrogen storage properties by hydride destabilization through alloy formation: LiH and MgH₂ destabilized with Si. *J. Phys. Chem. B* **108**(37), 13977–13983 (2004)
- R. Janot, F. Cuevas, M. Lacroche, A. Percheron-Guégan, Influence of crystallinity on the structural and hydrogenation properties of Mg₂X phases (X = Ni, Si, Ge, Sn). *Intermetallics* **14**(2), 163–169 (2006)
- J. Zhang, Z. Li, F. Cuevas, M. Lacroche, Phase stabilities in the Mg–Si–H system tuned by mechanochemistry. *J. Phys. Chem. C* **118**(38), 21889–21895 (2014)
- A.-L. Chaudhary, M. Paskevicius, D.A. Sheppard, C.E. Buckley, Thermodynamic destabilisation of MgH₂ and NaMgH₃ using Group IV elements Si, Ge or Sn. *J. Alloys Compd.* **623**, 109–116 (2015)
- M. Paskevicius, D.A. Sheppard, A.L. Chaudhary, C.J. Webb, E.M.A. Gray, H.Y. Tian, V.K. Peterson, C.E. Buckley, Kinetic limitations in the Mg–Si–H system. *Int. J. Hydrog. Energy* **36**(17), 10779–10786 (2011)
- A.-L. Chaudhary, D.A. Sheppard, M. Paskevicius, C.J. Webb, E.M. Gray, C.E. Buckley, Mg₂Si nanoparticle synthesis for high pressure hydrogenation. *J. Phys. Chem. C* **118**(2), 1240–1247 (2014)
- J. Bystrzycki, T. Płociński, W. Zieliński, Z. Wiśniewski, M. Polanski, W. Mróz, Z. Bojar, K.J. Kurzdłowski, Nano-engineering of magnesium hydride for hydrogen storage. *Microelectron. Eng.* **86**(4–6), 889–891 (2009)
- G.S. Walker, M. Abbas, D.M. Grant, C. Udeh, Destabilisation of magnesium hydride by germanium as a new potential multicomponent hydrogen storage system. *Chem. Commun.* **47**(28), 8001 (2011)
- F.C. Gennari, F.J. Castro, G. Urretavizcaya, G. Meyer, Catalytic effect of Ge on hydrogen desorption from MgH₂. *J. Alloys Compd.* **334**(1–2), 277–284 (2002)
- Abbas M. Thermodynamic Tuning of Light Metal Hydrides Multicomponent Systems by Ge [PhD Thesis]. University of Nottingham; 2014
- M. Polanski, J. Bystrzycki, The influence of different additives on the solid-state reaction of magnesium hydride (MgH₂) with Si. *Int. J. Hydrog. Energy* **34**(18), 7692–7699 (2009)
- A. Andreasen, M.B. Sørensen, R. Burkarl, B. Møller, A.M. Molenbroek, A.S. Pedersen, J.W. Andreasen, M.M. Nielsen, T.R. Jensen, Interaction of hydrogen with an Mg–Al alloy. *J. Alloys Compd.* **404–406**, 323–326 (2005)
- J.F. Fernández, C.R. Sánchez, Rate determining step in the absorption and desorption of hydrogen by magnesium. *J. Alloys Compd.* **340**(1–2), 189–198 (2002)
- J.F. Fernández, C.R. Sánchez, Simultaneous TDS–DSC measurements in magnesium hydride. *J. Alloys Compd.* **356–357**, 348–352 (2003)

27. G. Friedlmeier, M. Arakawa, T. Hirai, E. Akiba, Preparation and structural, thermal and hydriding characteristics of melt-spun Mg–Ni alloys. *J. Alloys Compd.* **292**(1–2), 107–117 (1999)
28. E. Callini, L. Pasquini, T.R. Jensen, E. Bonetti, Hydrogen storage properties of Mg–Ni nanoparticles. *Int. J. Hydrog. Energy* **38**(27), 12207–12212 (2013)
29. A. Zaluska, L. Zaluski, J.O. Ström-Olsen, Synergy of hydrogen sorption in ball-milled hydrides of Mg and Mg₂Ni. *J. Alloys Compd.* **289**(1–2), 197–206 (1999)
30. S. Orimo, Structural and hydriding properties of the Mg–Ni–H system with nano- and/or amorphous structures. *Acta Mater.* **45**(6), 2271–2278 (1997)
31. J. Matsuda, N. Uchiyama, T. Kanai, K. Harada, E. Akiba, Effect of Mg/Ni ratio on microstructure of Mg–Ni films deposited by magnetron sputtering. *J. Alloys Compd.* **617**, 47–51 (2014)
32. J. Matsuda, K. Yoshida, Y. Sasaki, N. Uchiyama, E. Akiba, In situ observation on hydrogenation of Mg–Ni films using environmental transmission electron microscope with aberration correction. *Appl. Phys. Lett.* **105**(8), 083903 (2014)
33. R. Bogerd, P. Adelhelm, J.H. Meeldijk, K.P. de Jong, P.E. de Jongh, The structural characterization and H₂ sorption properties of carbon-supported Mg_{1–x}Ni_x nanocrystallites. *Nanotechnology* **20**(20), 204019 (2009)
34. Y. Wu, M.V. Lototsky, J.K. Solberg, V.A. Yartys, Effect of microstructure on the phase composition and hydrogen absorption–desorption behaviour of melt-spun Mg–20Ni–8Mm alloys. *Int. J. Hydrog. Energy* **37**(2), 1495–1508 (2012)
35. S. Løken, J.K. Solberg, J.P. Maehlen, R.V. Denys, M.V. Lototsky, B.P. Tarasov, V.A. Yartys, Nanostructured Mg–Mm–Ni hydrogen storage alloy: structure–properties relationship. *J. Alloys Compd.* **446–447**, 114–120 (2007)
36. V.A. Yartys, V.E. Antonov, D. Chernyshov, J.C. Crivello, R.V. Denys, V.K. Fedotov, M. Gupta, V.I. Kulakov, M. Latroche, D. Sheptyakov, Structure and chemical bonding in MgNi₂H₃ from combined high resolution synchrotron and neutron diffraction studies and ab initio electronic structure calculations. *Acta Mater.* **98**, 416–422 (2015)
37. J.J. Reilly, R.H. Wiswall, Reaction of hydrogen with alloys of magnesium and copper. *Inorg. Chem.* **6**(12), 2220–2223 (1967)
38. A. Karty, Hydriding and dehydriding kinetics of Mg in a Mg/Mg₂Cu eutectic alloy: pressure sweep method. *J. Appl. Phys.* **50**(11), 7200 (1979)
39. A. Andreasen, M.B. Sørensen, R. Burkarl, B. Møller, A.M. Molenbroek, A.S. Pedersen, T. Vegge, T.R. Jensen, Dehydrogenation kinetics of air-exposed MgH₂/Mg₂Cu and MgH₂/MgCu₂ studied with in situ X-ray powder diffraction. *Appl. Phys. A* **82**(3), 515–521 (2006)
40. K.T. Møller, B.R.S. Hansen, A.-C. Dippel, J.-E. Jørgensen, T.R. Jensen, Characterization of gas–solid reactions using in situ powder X-ray diffraction. *Z. Anorg. Allg. Chem.* **640**(15), 3029–3043 (2014)
41. B.R.S. Hansen, K.T. Møller, M. Paskevicius, A.-C. Dippel, P. Walter, C.J. Webb, C. Pistidda, N. Bergemann, M. Dornheim, T. Klassen, J.-E. Jørgensen, T.R. Jensen, In situ X-ray diffraction environments for high-pressure reactions. *J. Appl. Crystallogr.* **48**(4), 1234–1241 (2015)
42. Y.S. Au, M. Ponthieu, R. van Zwielen, C. Zlotea, F. Cuevas, K.P. de Jong, P.E. de Jongh, Synthesis of Mg₂Cu nanoparticles on carbon supports with enhanced hydrogen sorption kinetics. *J. Mater. Chem. A* **1**(34), 9983 (2013)
43. M. Norek, T.K. Nielsen, M. Polanski, I. Kuncce, T. Płociński, L.R. Jaroszewicz, Y. Cerenius, T.R. Jensen, J. Bystrzycki, Synthesis and decomposition mechanisms of ternary Mg₂CoH₅ studied using in situ synchrotron X-ray diffraction. *Int. J. Hydrog. Energy* **36**(17), 10760–10770 (2011)
44. L. Pasquini, E. Callini, M. Brighi, F. Boscherini, A. Montone, T.R. Jensen, C. Maurizio, M.V. Antisari, E. Bonetti, Magnesium nanoparticles with transition metal decoration for hydrogen storage. *J. Nanopart. Res.* **13**(11), 5727–5737 (2011)
45. H. Shao, M. Felderhoff, F. Schüth, Hydrogen storage properties of nanostructured MgH₂/TiH₂ composite prepared by ball milling under high hydrogen pressure. *Int. J. Hydrog. Energy* **36**(17), 10828–10833 (2011)
46. M. Ponthieu, F. Cuevas, J.F. Fernández, L. Laversenne, F. Porcher, M. Latroche, Structural properties and reversible deuterium loading of MgD₂–TiD₂ Nanocomposites. *J. Phys. Chem. C* **117**(37), 18851–18862 (2013)
47. E. Callini, L. Pasquini, L.H. Rude, T.K. Nielsen, T.R. Jensen, E. Bonetti, Hydrogen storage and phase transformations in Mg–Pd nanoparticles. *J. Appl. Phys.* **108**(7), 073513 (2010)
48. M. Ponthieu, Y.S. Au, K. Provost, C. Zlotea, E. Leroy, J.F. Fernández, M. Latroche, P.E. de Jongh, F. Cuevas, Nanoconfinement of Mg₆Pd particles in porous carbon: size effects on structural and hydrogenation properties. *J. Mater. Chem. A* **2**(43), 18444–18453 (2014)
49. M. Polanski, T.K. Nielsen, Y. Cerenius, J. Bystrzycki, T.R. Jensen, Synthesis and decomposition mechanisms of Mg₂FeH₆ studied by in situ synchrotron X-ray diffraction and high-pressure DSC. *Int. J. Hydrog. Energy* **35**(8), 3578–3582 (2010)
50. M. Polanski, T. Płociński, I. Kuncce, J. Bystrzycki, Dynamic synthesis of ternary Mg₂FeH₆. *Int. J. Hydrog. Energy* **35**(3), 1257–1266 (2010)
51. S.S. Raman, D.J. Davidson, J.L. Bobet, O.N. Srivastava, Investigations on the synthesis, structural and microstructural characterizations of Mg-based K₂PtCl₆ type (Mg₂FeH₆) hydrogen storage material prepared by mechanical alloying. *J. Alloys Compd.* **333**(1–2), 282–290 (2002)
52. C. Milanese, A. Girella, G. Bruni, V. Berbenni, P. Cofrancesco, A. Marini, M. Villa, P. Matteazzi, Hydrogen storage in magnesium–metal mixtures: reversibility, kinetic aspects and phase analysis. *J. Alloys Compd.* **465**(1–2), 396–405 (2008)
53. T. Liu, T. Zhang, X. Zhang, X. Li, Synthesis and hydrogen storage properties of ultrafine Mg–Zn particles. *Int. J. Hydrog. Energy* **36**(5), 3515–3520 (2011)
54. S. Deledda, B.C. Hauback, H. Fjellvåg, H-sorption behaviour of mechanically activated Mg–Zn powders. *J. Alloys Compd.* **446–447**, 173–177 (2007)
55. T.A. Webb, C.J. Webb, A.K. Dahle, E.M. Gray, In-situ neutron powder diffraction study of Mg–Zn alloys during hydrogen cycling. *Int. J. Hydrog. Energy* **40**(25), 8106–8109 (2015)
56. D. Shechtman, I. Blech, D. Gratias, J.W. Cahn, Metallic phase with long-range orientational order and no translational symmetry. *Phys. Rev. Lett.* **53**(20), 1951–1953 (1984)
57. W. Steurer, S. Deloudi, Fascinating quasicrystals. *Acta Crystallogr. A* **64**(Pt 1), 1–11 (2008)
58. Z. Luo, S. Zhang, Y. Tang, D. Zhao, Quasicrystals in as-cast Mg–Zn–RE alloys. *Scr. Metall. Mater.* **28**(12), 1513–1518 (1993)
59. A. van Blaaderen, Materials science: quasicrystals from nanocrystals. *Nature* **461**(7266), 892–893 (2009)
60. A.M. Viano, R.M. Stroud, P.C. Gibbons, A.F. McDowell, M.S. Conradi, K.F. Kelton, Hydrogenation of titanium-based quasicrystals. *Phys. Rev. B: Condens. Matter* **51**(17), 12026–12029 (1995)
61. A.M. Viano, E.H. Majzoub, R.M. Stroud, M.J. Kramer, S.T. Mixture, P.C. Gibbons, K.F. Kelton, Hydrogen absorption and storage in quasicrystalline and related Ti–Zr–Ni alloys. *Philos. Mag. A* **78**(1), 131–142 (1998)
62. M. Sahlberg, Y. Andersson, Hydrogen absorption in Mg–Y–Zn ternary compounds. *J. Alloys Compd.* **446–447**, 134–137 (2007)
63. X. Luo, D.M. Grant, G.S. Walker, Hydrogen storage properties for Mg–Zn–Y quasicrystal and ternary alloys. *J. Alloys Compd.* **645**, S23–S26 (2015)

64. R.V. Denys, V.A. Yartys, Effect of magnesium on the crystal structure and thermodynamics of the $\text{La}_{3-x}\text{Mg}_x\text{Ni}_9$ hydrides. *J. Alloys Compd.* **509**, S540–S548 (2011)
65. R.V. Denys, V.A. Yartys, C.J. Webb, Hydrogen in $\text{La}_2\text{MgNi}_9\text{D}_{13}$: the role of magnesium. *Inorg. Chem.* **51**(7), 4231–4238 (2012)
66. V. Yartys, R. Denys, Structure–properties relationship in $\text{RE}_3 - x\text{Mg}_x\text{Ni}_9\text{H}_{10-13}$ (RE = La, Pr, Nd) hydrides for energy storage. *J. Alloys Compd.* **645**, S412–S418 (2015)
67. R. Denys, V. Yartys, E. Gray, C. Webb, LaNi_5 -assisted hydrogenation of MgNi_2 in the hybrid structures of $\text{La}_{1.09}\text{Mg}_{1.91}\text{Ni}_9\text{D}_{9.5}$ and $\text{La}_{0.91}\text{Mg}_{2.09}\text{Ni}_9\text{D}_{9.4}$. *Energies* **8**(4), 3198–3211 (2015)
68. Q. Lai, M. Paskevicius, D.A. Sheppard, C.E. Buckley, A.W. Thornton, M.R. Hill, Q. Gu, J. Mao, Z. Huang, H.K. Liu, Z. Guo, A. Banerjee, S. Chakraborty, R. Ahuja, K.-F. Aguey-Zinsou, Hydrogen storage materials for mobile and stationary applications: current state of the art. *ChemSusChem.* **8**(17), 2789–2825 (2015)
69. D.A. Sheppard, C. Corgnale, B. Hardy, T. Motyka, R. Zidan, M. Paskevicius, C.E. Buckley, Hydriding characteristics of NaMgH_2F with preliminary technical and cost evaluation of magnesium-based metal hydride materials for concentrating solar power thermal storage. *RSC Adv.* **4**(51), 26552–26562 (2014)
70. J.C. Crivello, J. Zhang, M. Latroche, Structural stability of ABy Phases in the (La, Mg)–Ni system obtained by density functional theory calculations. *J. Phys. Chem. C* **115**(51), 25470–25478 (2011)
71. J.-C. Crivello, M. Gupta, M. Latroche, First principles calculations of (La, Mg) $_2\text{Ni}_7$ hydrides. *J. Alloys Compd.* **645**, S5–S8 (2015)
72. V.A. Yartys, V.E. Antonov, A.I. Beskrovnyy, J.C. Crivello, R.V. Denys, V.K. Fedotov, M. Gupta, V.I. Kulakov, M.A. Kuzovnikov, M. Latroche, Y.G. Morozov, S.G. Sheverev, B.P. Tarasov, Hydrogen-assisted phase transition in a trihydride MgNi_2H_3 synthesized at high H_2 pressures: thermodynamics, crystallographic and electronic structures. *Acta Mater.* **82**, 316–327 (2015)
73. D.A. Sheppard, M. Paskevicius, T.D. Humphries, M. Felderhoff, G. Capurso, J. Bellosta von Colbe, M. Dornheim, T. Klassen, P.A. Ward, J.A. Teprovich Jr., C. Corgnale, R. Zidan, D.M. Grant, C.E. Buckley, Metal hydrides for concentrating solar-thermal power energy storage. *J. Appl. Phys. A* (in preparation)
74. J.-C. Crivello, B. Dam, R.V. Denys, M. Dornheim, D.M. Grant, J. Huot, T.R. Jensen, P. de Jongh, M. Latroche, C. Milanese, D. Milčius, G.S. Walker, C.J. Webb, C. Zlotea, V.A. Yartys, Review of magnesium hydride based materials: development and optimisation. *Appl. Phys. A*. doi:10.1007/s00339-016-9602-0
75. P. de Rango, P. Marty, D. Fruchart, Integrated with FC H storage systems utilising magnesium hydride: experimental studies and modelling. *Appl. Phys. A* (in preparation)